Title

Sources and photochemistry of volatile organic compounds in the remote atmosphere of western China: results from the Mt. Waliguan Observatory

Journal

Atmospheric Chemistry and Physics, 13(17)

ISSN

1680-7324

Authors

Xue, L. K
Wang, T.
Guo, H.
et al.

Publication Date

2013-09-02

DOI

10.5194/acp-13-8551-2013

Atmos. Chem. Phys., 13, 8551–8567, 2013
www.atmos-chem-phys.net/13/8551/2013/
doi:10.5194/acp-13-8551-2013

Atmospheric Chemistry and Physics Open Access

Sources and photochemistry of volatile organic compounds in the remote atmosphere of western China: results from the Mt. Waliguan Observatory

L. K. Xue[1,2], T. Wang[1,2], H. Guo[1], D. R. Blake[3], J. Tang[4], X. C. Zhang[4], S. M. Saunders[5], and W. X. Wang[2]

[1]Department of Civil and Environmental Engineering, Hong Kong Polytechnic University, Hong Kong, China
[2]Environmental Research Institute, Shandong University, Ji'nan, Shandong, China
[3]Department of Chemistry, University of California at Irvine, Irvine, CA, USA
[4]Center for Atmosphere Watch and Services, Key Laboratory for Atmospheric Chemistry, Chinese Academy of Meteorological Sciences, Beijing, China
[5]School of Chemistry and Biochemistry, the University of Western Australia, WA, Perth, Australia

Correspondence to: T. Wang (cetwang@polyu.edu.hk)

Received: 13 March 2013 – Published in Atmos. Chem. Phys. Discuss.: 2 May 2013
Revised: 9 July 2013 – Accepted: 17 July 2013 – Published: 2 September 2013

Abstract. The chemistry of the natural atmosphere and the influence by long-range transport of air pollution are key issues in the atmospheric sciences. Here we present two intensive field measurements of volatile organic compounds (VOCs) in late spring and summer of 2003 at Mt. Waliguan (WLG, 36.28° N, 100.90° E, 3816 m a.s.l.), a baseline station in the northeast part of the Qinghai-Tibetan Plateau. Most VOC species exhibited higher concentrations in late spring than in summer. A typical diurnal variation was observed with higher nighttime levels, in contrast to results from other mountainous sites. Five different air masses were identified from backward trajectory analysis showing distinct VOC speciation. Air masses originating from the central Eurasian continent contained the lowest VOC levels compared to the others that were impacted by anthropogenic emissions from China and the Indian subcontinent. A photochemical box model based on the Master Chemical Mechanism (version 3.2) and constrained by a full suite of measurements was developed to probe the photochemistry of atmosphere at WLG. Our results show net ozone production from in situ photochemistry during both late spring and summer. Oxidation of nitric oxide (NO) by the hydroperoxyl radical (HO_2) dominates the ozone production relative to the oxidation by the organic peroxy radicals (RO_2), and the ozone is primarily destroyed by photolysis and reactions with the HO_x ($HO_x = OH + HO_2$) radicals. Ozone photolysis is the predominant primary source of radicals ($RO_x = OH + HO_2 + RO_2$), followed by the photolysis of secondary oxygenated VOCs and hydrogen peroxides. The radical losses are governed by the self and cross reactions among the radicals. Overall, the findings of the present study provide insights into the background chemistry and the impacts of pollution transport on the pristine atmosphere over the Eurasian continent.

1 Introduction

Volatile organic compounds (VOCs) together with nitrogen oxides ($NO_x = NO + NO_2$) are key ingredients in the photochemical formation and fate of ozone (O_3) and other oxidants, which have great influence on atmospheric chemistry, regional air quality, and climate change (National Research Council, 1991; Crutzen, 1995). Tropospheric ozone originates primarily by downward transport from the stratosphere (Stohl et al., 2003), or from the in situ photochemical production involving CO, VOCs and NO_x (Crutzen, 1973). In the lower troposphere, the photochemistry plays a critical role in controlling the ozone budget (Crutzen, 1995). The photochemistry can act as either a source or a sink for ozone, depending on the abundances of NO_x. In NO_x-rich

environments, net ozone production can be achieved by the following simplified set of reactions.

$$\mathrm{VOC} + \mathrm{OH} \xrightarrow{\mathrm{O_2}} \mathrm{RO_2} + \mathrm{H_2O} \quad \text{(R1)}$$

$$\mathrm{CO} + \mathrm{OH} \xrightarrow{\mathrm{O_2}} \mathrm{HO_2} + \mathrm{CO_2} \quad \text{(R2)}$$

$$\mathrm{RO_2} + \mathrm{NO} \xrightarrow{\mathrm{O_2}} \mathrm{NO_2} + \mathrm{HO_2} + \text{carbonyls} \quad \text{(R3)}$$

$$\mathrm{HO_2} + \mathrm{NO} \rightarrow \mathrm{NO_2} + \mathrm{OH} \quad \text{(R4)}$$

$$\mathrm{NO_2} + h\nu\,(\lambda < 424\,\mathrm{nm}) \rightarrow \mathrm{NO} + \mathrm{O}(^3\mathrm{P}) \quad \text{(R5)}$$

$$\mathrm{O}(^3\mathrm{P}) + \mathrm{O_2} + \mathrm{M} \rightarrow \mathrm{O_3} + \mathrm{M} \quad \text{(R6)}$$

While in the remote atmosphere where NO levels are very low, the photochemical production of ozone cannot compensate for ozone destroyed by photolysis (R7-8) and reactions with hydroxyl (OH) and hydroperoxyl (HO_2) radicals (R9-10), resulting in net ozone destruction.

$$\mathrm{O_3} + h\nu\,(\lambda < 320\,\mathrm{nm}) \rightarrow \mathrm{O}(^1\mathrm{D}) + \mathrm{O_2} \quad \text{(R7)}$$

$$\mathrm{O}(^1\mathrm{D}) + \mathrm{H_2O} \rightarrow \mathrm{OH} + \mathrm{OH} \quad \text{(R8)}$$

$$\mathrm{OH} + \mathrm{O_3} \rightarrow \mathrm{HO_2} + \mathrm{O_2} \quad \text{(R9)}$$

$$\mathrm{HO_2} + \mathrm{O_3} \rightarrow \mathrm{OH} + 2\mathrm{O_2} \quad \text{(R10)}$$

Given the dual roles of photochemistry in the ozone budget, it is of great importance to conduct concurrent measurements of NO_x, CO and VOCs in order to quantify the role of photochemistry in the background atmosphere in different regions of the world.

Long-range transport of air pollution can significantly influence the composition and chemistry of the natural atmosphere. Extensive efforts have been made to understand the trans-Pacific transport of Asian air pollution, driven in part by concerns of the rapidly increasing emissions of air pollutants from eastern Asia (e.g., Akimoto et al., 1996; Jaffe et al., 1999; Jacob et al., 1999; Lin et al., 2010, 2012). One of these efforts was the NASA Transport and Chemical Evolution over the Pacific (TRACE-P) aircraft mission conducted in spring 2001, targeting the export of Asian continental air pollution to the Pacific Ocean (Jacob et al., 2003). Intercontinental transport of Asian pollution has been demonstrated to significantly affect the background levels of oxidants at the northern midlatitudes (Berntsen et al., 1999), and have potential impact on the air quality over continents downwind (e.g., Jacob et al., 1999; Lin et al., 2012). In comparison, there is little information about the westward transport of eastern Asian pollution and its impacts on chemistry of the remote atmosphere in the interior Eurasian continent. There are also relatively few studies on the transport from the upwind continents such as Europe to East Asia (e.g., Wild et al., 2004; HTAP, 2010; Lin et al., 2010). Consequently, it is necessary to consider these transport processes and understand their perturbation on the background atmosphere.

The Qinghai-Tibetan Plateau, located in the southwestern part of China, is the highest landmass on Earth, with an average altitude of over 4000 m above sea level (a.s.l.). Because of its unique geographic nature, the plateau is an ideal platform to study the chemistry of the background atmosphere and potential influences of pollution transport in the interior Asian continent. In 1994, China established its first (and to date the only) continental baseline atmospheric observatory at Mt. Waliguan (WLG; 36.28° N, 100.90° E, 3816 m a.s.l.), located on the northeastern edge of the plateau in Qinghai Province (Tang et al., 1995). Since then, greenhouse gases (including ozone) and aerosols have been measured continuously along with complete meteorological parameters (Tang et al., 1995; Ma et al., 2003; Zhou et al., 2003, 2004; Kivekäs et al., 2009). These observations have yielded valuable insight into the composition and chemistry of background atmosphere in the Asian continent. However, there are few measurements of ozone precursors, in particular VOCs, which are emitted from both natural and anthropogenic sources (Ma et al., 2002). Such information would provide valuable chemical evidence of the origins of air masses in this pristine continental atmosphere.

An unresolved scientific debate is the origin of elevated summertime surface ozone over the northeast Qinghai-Tibetan Plateau. Ozone concentrations exhibited a broad summer peak at WLG (Tang et al., 1995), which contrasts with the common spring maximum pattern in most remote areas of the Northern Hemisphere (Monks, 2000). Many follow-up studies have debated whether pollution transport or stratospheric intrusion plays a more dominant role (Zhu et al., 2004; Ma et al., 2005; Wang et al., 2006; Ding and Wang, 2006; Li et al., 2009; Xue et al., 2011). An analysis of backward trajectories for summers of 2000–2009 suggests the dominance of transport of anthropogenic pollution from central and eastern China in most years, but also indicates considerable contribution of stratospheric intrusions (Xue et al., 2011). Another debate is on the role of in situ photochemistry in the chemical ozone budget. Ma et al. (2002) applied a chemical box model to estimate the ozone budget at WLG and indicated a net destruction due to photochemistry in summer. In that study, ambient NO concentrations were not directly measured but estimated from filter-based measurements of NO_2. Subsequent in situ measurements of NO (the data to be used in the present study) implied a net ozone production (Wang et al., 2006). Evidently, a detailed analysis of the ozone chemical budget would need concurrent measurements of NO, CO and VOCs.

In April–May and July–August 2003 two intensive field studies, representing spring and summer seasons, were performed at WLG. A suite of air pollutants including O_3, CO, NO, NO_y, VOCs, and meteorological parameters were measured. The measurement results of O_3, CO and NO_y during the campaigns have been reported by Wang et al. (2006). In this paper, we present the measurements of VOCs. We first show the temporal variations of various VOC species and

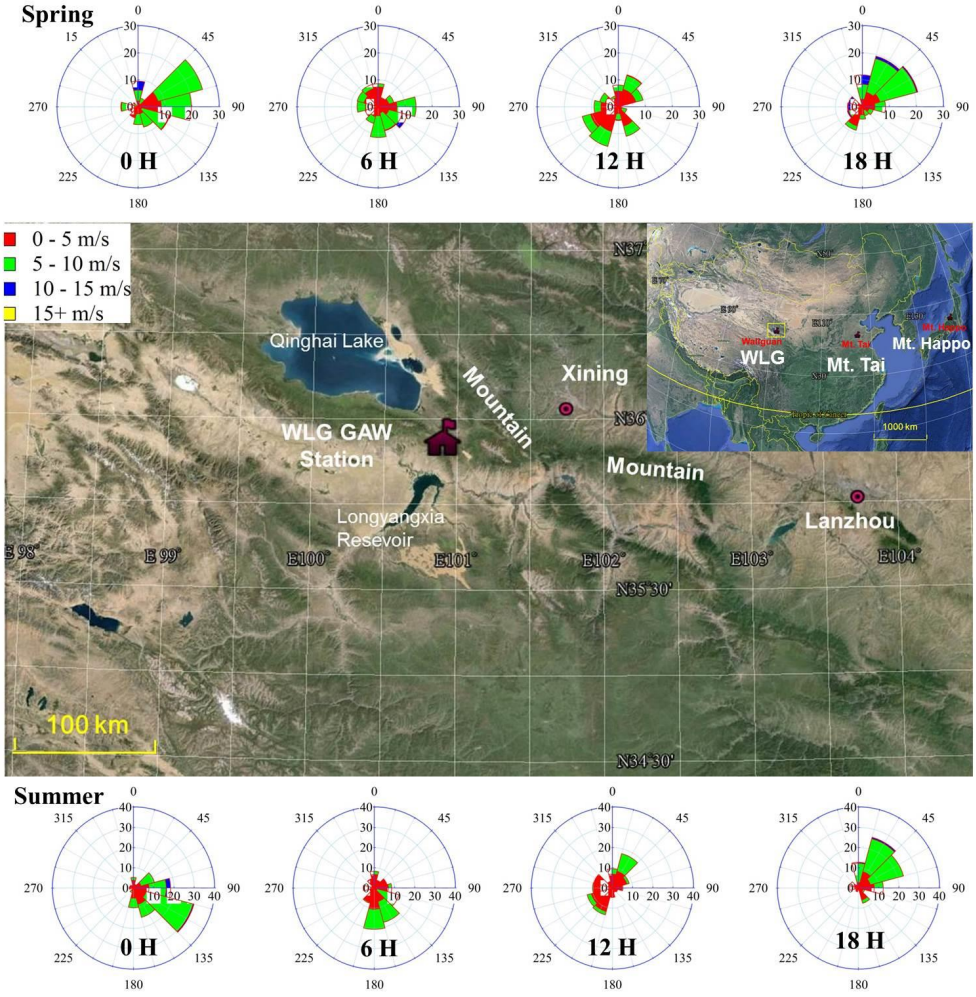

Fig. 1. Map from Google Earth showing the WLG Observatory and surrounding areas. The main figure is the zoomed view of the yellow box in the inner map. The diurnal variations of surface wind recorded in spring and summer are also shown.

make comparison with other remote stations at the northern midlatitudes (Sect. 3.1). We then apply the back trajectory techniques to classify the air parcels and examine the VOC speciation in different air masses (Sect. 3.2). Finally, the observational data set is used to constrain a chemical box model to understand the photochemistry of this background environment, including the budgets of ozone and radicals (Sect. 3.3).

2 Methods

2.1 Observations

The field campaigns were carried out at the WLG Observatory, which is one of the World Meteorological Organization's (WMO) Global Atmospheric Watch (GAW) baseline stations. The observatory has been used in many field studies, and has been described in detail elsewhere (e.g., Ma et al., 2003; Wang et al., 2006). Briefly, the station is situated on an isolated peak in the northeastern part of the Qinghai-Tibetan Plateau. It is relatively isolated from the industrialized and populated areas, with the population density less than 6 people per square kilometer (Zhou et al., 2003). The surrounding area has maintained its natural arid/semi-arid lands and scattered grasslands. The major anthropogenic emission sources nearby are located to the northeast and east (Fig. 1). Xining, the capital of Qinghai Province, is about 90 km northeast of the station, with several high mountains (∼ 4000 m a.s.l.) in between. To the east about 260 km is Lanzhou city, the capital of Gansu Province. A small town with a population of ∼ 30 000 and light industry is located about 26 km to the west, and a few agricultural counties with very sparse population are located to the south.

Two phases of intensive measurements were conducted from 20 April to 22 May and from 15 July to 16 August 2003, which aimed at studying the impacts of non-local sources

in spring and summer. Two-liter electro-polished stainless steel canisters, previously cleaned and evacuated at the University of California, Irvine (UCI), were used for sampling VOCs. The sampling inlet was installed at 3 m above the rooftop of the station. During the sampling, whole air was drawn through a stainless steel tube by a metal bellows pump and pressurized into the canisters to 24 psig. After the campaign, the canisters were shipped to UCI's laboratory for chemical analysis. A 5-column multiple GC system equipped with flame ionization detection (FID), electron capture detection (ECD) and mass spectrometer detection (MSD) was employed to identify and quantify the VOCs species. Detailed descriptions of the canister preparation, chemical analysis, quality assurance and control, and measurement precision and accuracy for each species are given by Blake et al. (1994) and Simpson et al. (2010). Normally, two samples were collected each day, one at noon ($\sim$ 12:00 LT) and one at midnight ($\sim$ 00:00 LT), representing the well-mixed air masses in the planetary boundary layer and in the free troposphere, respectively. A total of 63 and 52 canister samples were taken during the spring and summer phases.

O_3, CO and NO were measured in real-time with a time resolution of 1 min during the observation periods. The sampling system, instruments, calibration, measurement precision and uncertainties of these measurements have been described in detail by Wang et al. (2006). In addition, meteorological parameters including temperature, pressure, relative humidity, and horizontal and vertical winds, were routinely measured at a time resolution of 5 min at the observatory.

2.2 Backward trajectory analysis

Backward trajectory analysis is a useful tool to track the transport history of air masses (Russo et al., 2003; Wang et al., 2006). In the present study, we utilized the Hybrid Single Particle Lagrangian Integrated Trajectory model (HYSPLIT, version 4.8) developed by the National Oceanic and Atmospheric Administration (NOAA) Air Resources Laboratory (ARL) (http://ready.arl.noaa.gov/HYSPLIT.php) to calculate three-dimensional backward trajectories. The meteorological input is the National Centers for Environmental Prediction (NCEP) FNL data with a spatial resolution of 191 km $\times$ 191 km and a temporal frequency of 6 h, which is widely used to predict the large-scale meteorological conditions and transport (Gangoiti et al., 2006; Lin et al., 2009). Considering the high wind speeds at mountainous sites and relatively short lifetimes of many VOC species, we chose to compute back trajectories for 5 days. Two trajectories were determined each day at the sampling hours with the ending points at 500 m above the ground of the station. A total of 115 trajectories were then classified into five groups according to the directions from which the trajectories came (i.e., north, southeast, northwest, and southwest) as well as the altitudes where the trajectories passed before arriving at WLG (i.e., boundary layer and middle troposphere). A detailed description of the five trajectory groups is provided in Sect. 3.2. It is noteworthy that these five trajectory categories agree excellently with the transport pattern for the whole campaigns from cluster analysis of trajectories with high-resolution meteorological data (Wang et al., 2006).

2.3 Chemical box model

An observation-constrained photochemical box model was developed to probe into the chemistry of this background atmospheric environment. The model is configured based on the Master Chemical Mechanism (MCM, version 3.2; http://mcm.leeds.ac.uk/MCM/), which is a state-of-the-art chemical mechanism explicitly describing the degradation of 143 primary VOCs, comprising $\sim$ 16 900 reactions of $\sim$ 5725 organic species plus the latest inorganic mechanism from the IUPAC (International Union of Pure and Applied Chemistry) evaluation (Jenkin et al., 1997, 2003; Saunders et al., 2003). In addition to this "complete" gas phase chemistry, heterogeneous processes regarding nitrous acid (HONO) formation and HO_2 loss were also taken into account in the model. We adopted the parameterizations of Li et al. (2010) for HONO formation from heterogeneous reactions of NO_2 on both ground and aerosol surfaces. As to losses of HO_2 on aerosols, the parameterization used by Edwards et al. (2011) was incorporated. The aerosol surface area concentration and area-weighted radius, two key parameters in both parameterizations, were not measured during our studies. They were derived from the long-term measurements of aerosol number size distributions at WLG (Kivekäs et al., 2009), and constant aerosol surface of 7.1×10^{-5} m^2 m^{-3} and radius of 5.6×10^{-6} cm were used for both campaigns. Considering the facts that there was more anthropogenic influence (hence primary particles) at WLG in spring and at night but more extensive new particle formation (hence secondary particles) in summer and during the day (Wang et al., 2006; Kivekäs et al., 2009), the assumption of constant aerosol surface and radius should be somewhat reasonable. It is also noteworthy that the related uptake coefficients are still quite uncertain and may be highly variable depending on temperature and aerosol components (Thornton et al., 2008; Li et al., 2010), hence sensitivity of the model output to these processes was tested (see Sect. 3.3.1).

The photolysis frequencies appropriate for WLG and the seasons were parameterized using a two stream isotropic scattering model under clear sky conditions, and were calculated as a function of solar zenith angle within the model (Hayman, 1997; Saunders et al., 2003). Sensitivity studies were performed to examine the effect of potential clouds and aerosols on the modeling results (see Sect. 3.3.1). Dry deposition velocities of various inorganic gases, peroxy acetyl nitrates (PANs), peroxides, carbonyls and acids were adopted in the model from the recent compilation (Zhang et al., 2003). The mixing layer height was assumed to vary from 300 m at night to 1500 m in the afternoon in

the base simulations. Sensitivity analyses with varying maximum mixing heights were also conducted (see Sect. 3.3.1).

In the present study, two sets of simulations were carried out for the spring and summer campaigns, respectively. The campaign-median diurnal profiles of O_3, CO, NO, methane, 35 major non-methane hydrocarbons (see Table 1 for the species), temperature, pressure, and relative humidity were used as inputs. The model was constrained every ten minutes by the measurement data to calculate the reaction rates of interest. For VOC species which were only measured at noon and midnight, the concentrations were assumed to be constant during the day (08:00–19:50 LT) and at night (20:00–07:50 LT), respectively. This should be reasonable according to the less-varied diurnal profiles of CO at WLG (Wang et al., 2006). The initial time of the model run was set as 00:00 LT on 1 May 2003 (for spring) and 1 August 2003 (for summer). Each simulation was performed for ten days to stabilize the intermediate products not prescribed in the model (e.g., NO_2, radicals and oxygenated VOCs (OVOCs)), and the output of the tenth day was used for the analysis. Therefore, the OVOC species were just simulated in the model with constraints of VOC precursors and were only of secondary origin.

3 Results and discussion

3.1 Temporal variation and comparison with other studies

3.1.1 Temporal variations

Table 1 documents the statistics of major VOC species measured at WLG during the spring and summer campaigns. Overall inspection of data revealed that the levels of VOCs were relatively low, indicative of the background nature of the atmosphere. Three different types of seasonal behaviors were found although the field measurements in the present study were only conducted in two seasons. A typical pattern with higher concentrations in late spring and lower values in summer was observed for most species. This is consistent with the seasonal trends of CO and NO_y during the same observations (Wang et al., 2006), and is also in line with other studies conducted in remote areas at the northern midlatitudes (e.g., Rudolph, 1995; Atlas and Ridley, 1996; Klemp et al., 1997). Such patterns can be attributed to the seasonal variation of the atmospheric oxidative capacity, as confirmed by the higher levels of RO_x ($RO_x = OH + HO_2 + RO_2$) radicals in summer than in spring (see Sect. 3.3.2 and Fig. 7). For *i*-pentane and light olefins (i.e., ethene and propene), comparable and even slightly higher concentrations were detected in summer compared to those in spring. Given their relatively short lifetimes, this implied existence of local/nearby emission sources of these compounds with enhanced source strength in summer. Isoprene exhibited a pronounced pattern with much higher abundances in summer than in spring. This pattern is directly linked to the higher temperature and more intense solar radiation in summer, as the predominant biogenic source strength is known to increase with temperature and radiation (Guenther et al., 1997).

Figure 2 shows the diurnal variations of eight selected representative VOC species for both measurement campaigns. For combustion tracers (i.e., ethyne, benzene and methyl chloride (CH_3Cl)), and ethane and ethene, typical diurnal profiles of higher nighttime mixing ratios with lower daytime concentrations were determined. This pattern was also the case for most of the other species (figures not shown), and consistent with the diurnal variations of CO during the same studies (Wang et al., 2006). Such diurnal variation of air pollutants is opposite to those observed at other mountainous sites, which generally show higher daytime and lower nighttime levels driven by the mountain–valley breezes (Zaveri et al., 1995; Fischer et al., 1998, 2003; Zellweger et al., 2000; Carpenter et al., 2000). As a mountaintop site, WLG is also affected by mountain–valley breezes, with local anabatic and catabatic winds clearly observed during the observations (Wang et al., 2006; Xue et al., 2011). However, the daytime upslope flow of boundary-layer air and nighttime downslope flow of free tropospheric air resulted in a reversed diurnal variation of trace gases at WLG. This unusual phenomenon could be explained by transport of anthropogenic pollution during the night. This is illustrated by the diurnal variations of surface winds recorded at the observatory, as shown in Fig. 1. In spring, the surface winds were mainly from the southeast or northwest with relatively low speeds in the morning, and became calm at noon when the daytime canister samples were collected. In the evening, the winds switched to the northeast/east directions with higher speeds till midnight when the nighttime samples were taken. A similar diurnal pattern of surface winds was also observed in summer. Therefore, transport of anthropogenic pollution from the northeast/east, where Xining and Lanzhou are located, is likely responsible for the enhanced levels of CO and VOCs during the nighttime at WLG.

There were some exceptions to the aforementioned general diurnal pattern. Isoprene and *i*-pentane presented a diurnal profile with higher daytime and lower nighttime concentrations. For toluene and other reactive aromatics (e.g., ethylbenzene, xylenes and trimethylbenzenes; figures are not shown), the daytime concentrations were comparable to or slightly higher than those at night. These exceptions are consistent with the fact that the source strengths of these species are stronger during the daytime since their emissions are related with temperature. *i*-pentane is usually recognized as a tracer of gasoline evaporation (Morikawa et al., 1998). The aromatic hydrocarbons are known as main components of solvent usage (Guo et al., 2006). Thus gasoline spillage processes and solvent usage activities in surrounding areas (maybe the neighboring counties and towns) should be important contributors to the relatively elevated daytime levels of *i*-pentane and aromatics at WLG.

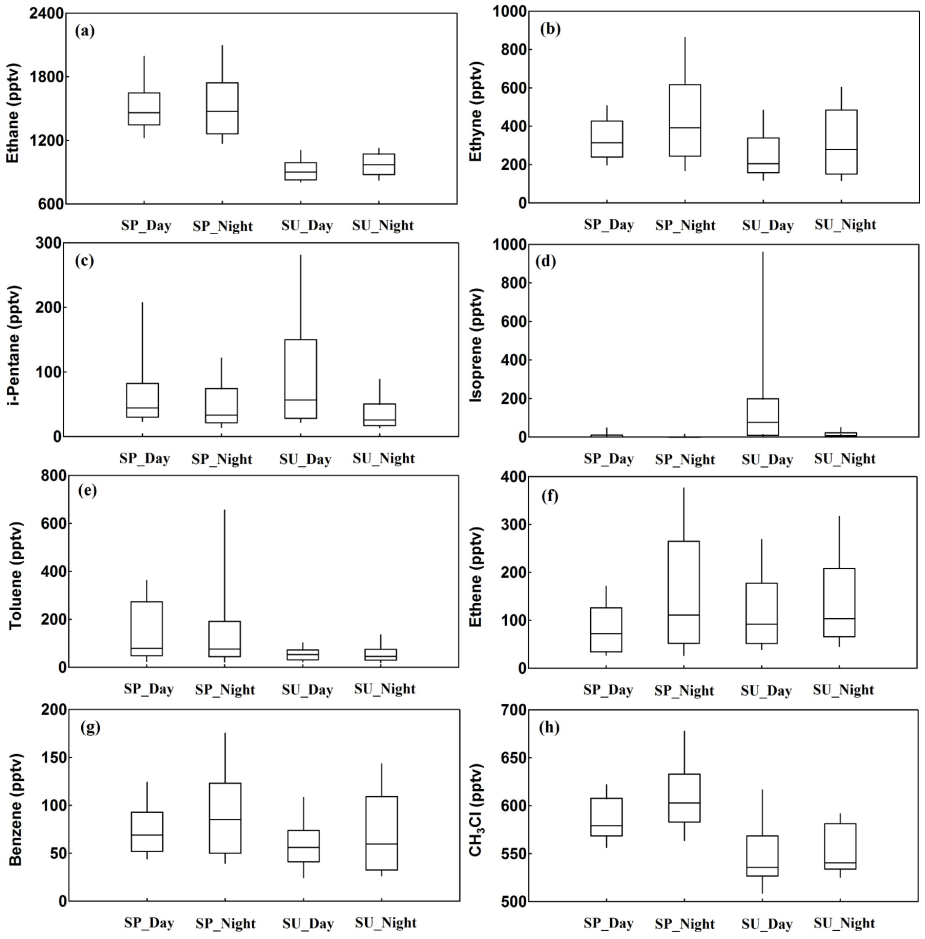

Fig. 2. Diurnal patterns of **(a)** ethane, **(b)** ethyne, **(c)** *i*-pentane, **(d)** isoprene, **(e)** toluene, **(f)** ethene, **(g)** benzene, and **(h)** CH_3Cl at WLG in spring (SP) and summer (SU). The box plot gives the 90th, 75th, 50th, 25th, and 10th percentiles of the measurement data.

3.1.2 Comparison with other midlatitude remote locations

It is of interest to compare the levels of VOCs at WLG with those from other remote areas across the northern midlatitudes. Table 2 summarizes the mean levels of major VOC species measured at WLG (this study, 3816 m), Jungfraujoch (Switzerland, 3580 m), Mt. Cimone (Italy, 2165 m), Mt. Tai (China, 1534 m), Happo (Japan, 1840 m), Mauna Loa (Hawaii, United States, 3400 m), and Izana (Spain, 2370 m). Jungfraujoch and Mt. Cimone are GAW stations in Europe, representing background conditions of the European continent. Mt. Tai and Happo are regional background stations in East Asia, with Mt. Tai located in the highly polluted region of the North China Plain (Suthawaree et al., 2010). Mauna Loa and Izana are representative high-elevation sites in the Pacific and Atlantic oceans, respectively, and thus can reflect background conditions of the marine atmosphere.

Overall, the springtime VOC levels at WLG were significantly lower than those measured at Jungfraujoch. Compared with Mt. Cimone, the summertime levels of ethane, benzene, and ethyne at WLG were comparable or slightly higher. For short-lived species, however, the abundances at WLG were much lower, with the exception of isoprene that is influenced by local vegetation. This suggests a cleaner continental background condition of WLG than the European continent. Compared to WLG, much higher levels of VOCs were observed at Happo and in particular at Mt. Tai, indicating the strong influence of anthropogenic emissions from eastern China and Japan. In comparison, much lower VOC levels were observed at Izana and Mauna Loa, reflecting the fact that the marine atmosphere is less impacted by anthropogenic pollution and has clearer background conditions.

3.2 Air mass transport and VOC speciation

Transport of air pollution is an important factor affecting the chemical composition of air parcels at remote locations. In order to understand the impact of long-range transport on the measured VOC levels at WLG, we calculated 5 day backward trajectories corresponding to the VOC sampling, and derived five types of air masses according to the transport

Table 1. Statistics of major VOC species measured at WLG[a].

	Species[b]	Spring ($n = 63$)			Summer ($n = 52$)		
		Mean	SD	Median	Mean	SD	Median
Alkanes	Methane	1.82	0.02	1.82	1.83	0.01	1.82
	Ethane	1532	308	1473	947	115	921
	Propane	279	111	259	147	45	137
	n-butane	67.9	35.6	54.0	40.1	19.9	35.0
	i-butane	54.7	44.8	40.0	30.2	18.2	27.0
	n-pentane	22.1	14.2	16.0	16.9	10.1	14.0
	i-pentane	63.4	56.6	39.0	68.8	81.5	40.0
	n-hexane	9.9	7.2	8.0	7.1	7.3	6.0
	2,2-dimethylbutane	3.5	3.1	4.0	–	–	–
	2-methylpentane	11.1	13.3	6.0	13.3	10.4	10.0
	3-methylpentane	4.3	4.3	4.0	–	–	–
	Cyclohexane	4.4	3.1	4.0	–	–	–
	n-heptane	7.9	7.5	6.0	5.5	4.5	5.0
	n-octane	5.6	6.1	4.0	5.7	2.2	5.0
	n-nonane	6.0	7.1	4.0	–	–	–
	n-decane	14.1	18.9	8.0	–	–	–
Alkenes	Ethene	131	145	95	138	111	97
	Propene	25.5	24.3	17.0	29.8	23.0	24.5
	1-butene	8.4	7.1	7.0	6.0	8.3	–
	i-butene	21.3	36.2	11.0	8.6	9.6	8.0
	Isoprene	5.7	16.1	–	126	287	16.0
	α-pinene	6.8	7.6	4.0	–	–	–
	β-pinene	6.7	7.8	5.0	–	–	–
Alkyne	Ethyne	392	204	358	293	182	232
Aromatics	Benzene	86.5	47.1	76.0	67.8	41.8	56.6
	Toluene	184	275	76.0	62.3	62.5	49.5
	Ethylbenzene	24.0	40.4	8.0	7.1	6.1	6.0
	m-xylene	69.1	137	14.0	14.1	10.2	10.0
	p-xylene	50.9	110	6.0	–	–	–
	o-xylene	45.7	81.4	10.0	9.4	7.4	8.0
	m-ethyltoluene	6.8	12.1	3.0	–	–	–
	p-ethyltoluene	3.8	6.9	–	–	–	–
	o-ethyltoluene	3.1	5.9	–	–	–	–
	1,2,3-trimethylbenzene	14.7	23.6	6.0	5.7	4.9	4.0
	1,2,4-trimethylbenzene	21.8	36.1	9.0	5.9	4.8	5.0
	1,3,5-trimethylbenzene	10.1	15.9	6.0	–	–	–
Halo-carbons	CH_3Cl	599	37	591	552	33	540
	C_2Cl_4	8.7	2.8	8.0	5.0	1.2	5.0

[a] Units are pptv, except for methane which is in ppmv; "–" denotes the values below detection limit, 3 pptv.
[b] All of these species were used to constrain the MCM box model.

pathways of trajectories. Figure 3 shows the representative trajectories of the five air mass categories identified. Here we name them by the directions from which the air parcels originated, and make a brief description as follows. Type North, air masses originated from Siberia or Mongolia and passing over inland northern China in the lower troposphere; type NW, air masses originated from the remote central Eurasian continent and traveling in the lower troposphere; type NW-MT, air masses from the western/central Eurasian continent and traveling at high speeds in the middle troposphere; type SW, air masses originated from India and climbing over the Qinghai-Tibetan Plateau; and type SE, air masses passing over southern and central China at lower altitudes before reaching the site. In spring, most of the samples corresponded with the air mass categories North (~ 40 %) and NW (~ 32 %), followed by NW-MT (~ 11 %), SE (~ 10 %), and SW (~ 8 %). In summer, the sample distribution of air masses was SE (~ 46 %), NW (~ 33 %), NW-MT (~ 12 %),

Table 2. Comparison of major hydrocarbon levels at WLG with observations at other mountain sites[a].

Species	Waliguan[b]		Jungfraujoch[c]	Mt. Cimone[d]	Mt. Tai[e]	Happo[f]		Mauna Loa[g]		Izana[h]
	Spring	Summer	Spring	Summer	Summer	Spring	Autumn	Spring	Summer	Summer
Ethane	1532 (308)	947 (115)	1755 (257)	905 (200)	2401 (778)	1741 (670)	749 (268)	1027 (200)	466 (121)	501 (113)
Propane	279 (111)	147 (45)	644 (981)	268 (110)	620 (331)	613 (340)	370 (219)	76 (44)	19 (11)	52 (38)
n-butane	68 (36)	40 (20)	159 (84)	108 (68)	209 (141)	223 (101)	103 (21)	8.5 (10.6)	1.5 (1.7)	22 (31)
i-butane	55 (45)	30 (19)	88 (52)	96 (50)	157 (87)	131 (65)	55 (14)	4.5 (4.9)	0.4 (6)	14 (30)
n-pentane	22 (14)	17 (10)	50 (37)	35 (26)	85 (53)	81 (29)	49 (9)	1.8 (2.2)	0.6 (0.3)	14 (25)
i-pentane	63 (57)	69 (81)	116 (108)	n.a.	172 (96)	112 (49)	67 (15)	n.a.	n.a.	14 (30)
Ethene	131 (145)	138 (111)	n.a.	261 (120)	994 (723)	208 (86)	296 (105)	4.5 (1.7)	3.5 (3)	35 (20)
Propene	26 (24)	30 (23)	52 (32)	75 (39)	110 (47)	61 (19)	101 (78)	2.8 (1.2)	1.9 (1.8)	10 (4)
Isoprene	6 (16)	126 (287)	n.a.	111 (124)	173 (184)	n.a.	343 (158)	0.2 (0.6)	0.7 (3.1)	60 (124)
Ethyne	392 (204)	293 (182)	567 (242)	201 (102)	1609 (969)	696 (80)	804 (471)	231 (69)	33 (22)	52 (30)
Benzene	87 (47)	68 (42)	148 (54)	65 (33)	641 (349)	n.a.	n.a.	33.4 (17.7)	7.1 (3.2)	27 (24)
Toluene	184 (275)	62 (62)	184 (156)	n.a.	205 (123)	n.a.	n.a.	1.1 (1.1)	0.3 (0.3)	26 (38)

[a] All data are mean values (standard deviation) in pptv. [b] Waliguan: 36.28° N, 100.90° E, 3816 m a.s.l.; Spring: 20 April–22 May 2003; Summer: 15 July–12 August 2003. This study. [c] Jungfraujoch: 46.55° N, 7.99° E, 3580 m a.s.l.; Spring: 25 March–13 April 1998; Carpenter et al., 2000. [d] Mt. Cimone: 44.18° N, 10.70° E, 2165 m a.s.l.; Summer: June–July 2000; Fischer et al., 2003. [e] Mt. Tai: 36.26° N, 117.11° E, 1534 m a.s.l.; Summer: June 2006; Suthawaree et al., 2010. [f] Happo: 36.68° N, 137.80° E, 1840 m a.s.l.; a whole-year measurement from March 1998–February 1999 was made; Sharma et al., 2000. [g] Mauna Loa: 19.54° N, 155.58° E, 3400 m a.s.l.; Spring: 15 April–15 May 1992; Summer: 15 July–15 August 1992; Atlas and Ridley, 1996. [h] Izana: 28.31° N, 16.50° W, 2370 m a.s.l., Summer: 31 July–22 August 1993. Only daytime data are used; Fischer et al., 1998.

Table 3. Classification results of CO and selected long-lived VOCs in different air mass groups at WLG[a].

Species	Spring					Summer		
	North[b] ($n=20$)	NW ($n=25$)	SE ($n=6$)	SW ($n=5$)	NW-MT ($n=7$)	NW ($n=17$)	SE ($n=24$)	NW-MT ($n=6$)
CO	153 (44)	133 (27)	152 (31)	150 (21)	111 (14)	93 (9)	125 (25)	113 (24)
Ethane	1743 (348)	1427 (230)	1560 (267)	1547 (243)	1266 (79)	943 (100)	949 (119)	874 (107)
Propane	343 (129)	248 (69)	334 (114)	273 (122)	166 (21)	125 (35)	167 (45)	116 (30)
n-butane	87 (42)	60 (26)	86 (30)	59 (31)	32 (7)	27 (12)	49 (22)	34 (14)
i-butane	62 (34)	59 (60)	64 (22)	42 (25)	20 (5)	17 (8)	39 (21)	23 (13)
Ethyne	443 (233)	353 (165)	548 (251)	453 (140)	214 (75)	152 (67)	370 (162)	280 (129)
Benzene	100 (61)	76 (32)	121 (46)	99 (34)	48 (14)	35 (15)	84 (36)	65 (29)
CH_3Cl	601 (40)	589 (35)	627 (42)	627 (23)	588 (16)	539 (30)	558 (29)	559 (26)
C_2Cl_4	9.6 (3.0)	8.2 (2.6)	9.5 (3.8)	8.0 (2.8)	7.4 (1.3)	4.9 (1.1)	5.1 (1.3)	4.8 (0.8)

[a] Values are mean concentrations (standard deviation) in pptv; CO is given in ppbv. [b] See text and Fig. 3 for the description of the air mass groups.

North (∼ 6 %), and SW (∼ 4 %). These transport patterns were consistent with those determined for the entire measurement campaign (Wang et al., 2006), and also agreed with the climatological summertime transport pattern at WLG (Xue et al., 2011). Also shown in Fig. 3 is the anthropogenic VOC emissions in the Asian region (Zhang et al., 2009), from which we can see that the emissions are concentrated in eastern China and northern India and are very low in the western part.

The VOC speciation within different air masses was then evaluated. Considering the losses of VOCs during transport, here we only took into account the species with relatively long lifetimes (i.e., ≥ 5 days). Table 3 documents the statistics of CO and major long-lived VOC species in different air masses for both campaigns. (Note that results were not obtained for types North and SW in summer due to the low sampling frequencies.) Overall inspection indicated that the levels of CO and VOCs in air masses NW and NW-MT were much lower than those in the other three categories. This is consistent with the fact that NW and NW-MT mostly came from the lower and middle troposphere over the central Eurasian continent, a large remote region with very few anthropogenic emissions. Relatively higher VOC levels in types North, SW and SE in spring indicated influences of anthropogenic emissions from specific regions over which the air parcels had passed. For example, the type North air masses may be influenced by anthropogenic emissions over northern China, as along the trajectories are located several large cities such as Yinchuan (the capital of Ningxia Autonomous Region) and Xining. The air masses SE and SW should have picked up the anthropogenic pollution in eastern or central China and northern India.

Here of interest is that the distributions in concentration of VOCs were different for the three air masses, although the levels of CO were similar. Type North contained the highest levels of ethane (1743 ± 348 pptv) and propane

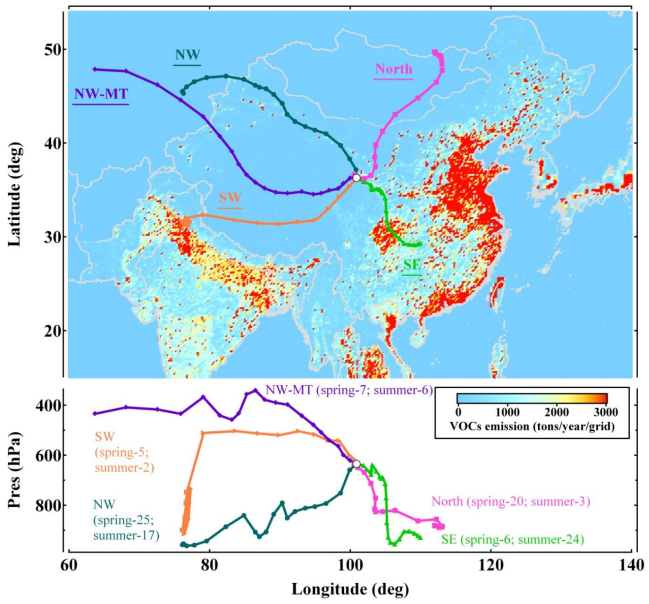

Fig. 3. Five types of air masses classified by the 5 d backward trajectories at WLG.

(343 ± 129 pptv), indicative of signature of natural gas leakage along the transport pathway. In comparison, type SE had the most abundances of ethyne (548 ± 251 pptv), benzene (121 ± 46 pptv) and CH_3Cl (627 ± 42 pptv), which are primarily emitted from the combustion of fossil fuels or biomass/biofuel. Both air masses also showed the highest concentrations of C_2Cl_4 (9.5–9.6 pptv), a tracer for urban or industrial activities (Wang et al., 1995). The mean mixing ratio of CH_3Cl (627 ± 23 pptv) in type SW was among the highest, although the levels of other VOC species were relatively lower. CH_3Cl is usually recognized as a tracer for biomass/biofuel burning (Blake et al., 2003), so the results may reflect the importance of biomass/biofuel combustion in India or southwestern China.

3.3 Daytime photochemistry

In this section, the daytime photochemistry of the natural continental atmosphere at WLG is explored with the aid of a photochemical box model constrained by a full suite of in situ measurements (see Sect. 2.3). The issues of interest are (1) what is the role of atmospheric photochemistry in the chemical ozone budget, and (2) what is the feedback of ozone on the atmospheric oxidation chemistry? Answers to these questions were probed by estimating the chemical budgets of ozone and RO_x radicals as described below.

3.3.1 In situ ozone production

The in situ photochemical production and destruction rates of ozone were calculated by the model. The ozone production is mainly achieved through the oxidation of NO by HO_2 and RO_2 (R3 and R4), and the production rate (Pls. keep $P(O_3)$) can be calculated as

$$P(O_3) = k_4[HO_2][NO] + \sum(k_{3i}[RO_2]_i[NO]). \quad (1)$$

In addition to the photolysis and reactions with HO_x ($HO_x = OH + HO_2$) (R7-10), ozone can be also chemically destroyed by the reactions with unsaturated VOCs (R11).

$$O_3 + \text{unsat. VOCs} = \text{carbonyls} + \text{Criegee biradicals} \quad (R11)$$

Thus, the ozone destruction rate can be described as

$$D(O_3) = k_8\left[O(^1D)\right][H_2O] + k_9[OH][O_3] + k_{10}[HO_2][O_3] + \sum(k_{11i}[VOC_i])[O_3]. \quad (2)$$

Then the net ozone production rate can be determined as the difference between Eqs. (1) and (2).

Figure 4 shows the campaign-median diurnal variations of ozone production, destruction, and net rates at WLG calculated by the model. It can be seen that the ozone production was significantly greater than the ozone destruction during the daytime in both spring and summer, indicative of net ozone production in both seasons. The daytime average net production rates were estimated as 0.31 and 0.26 ppb h^{-1} in spring and summer, respectively, indicating that 3.7 and 3.4 ppb of ozone can be formed from the in situ photochemistry in the course of one day. Such amounts were of the same magnitude as the observed ozone increases of 4–5 ppb from early morning to late afternoon at WLG (Wang et al., 2006). Thus, the in situ photochemical production should be an important factor in shaping the daytime accumulation of surface ozone at WLG.

This result is in disagreement with the previous modeling work by Ma et al. (2002) that suggested a net ozone production in winter but a net destruction in summer at WLG. Examination of model parameters revealed three major differences between the two studies. First, the concentrations of non-methane hydrocarbons (NMHCs), in particular alkenes and alkanes (except ethane), were much higher in the previous study. An extreme case is ethene, the mean concentration of which was 2.23 ppbv in Ma et al. (2002) (such a high level is usually observed in polluted environments) compared to 0.10 ppbv (campaign median) in ours. The reason for this discrepancy was unclear. Nonetheless, the difference in NMHC concentrations is not believed to be the cause of the contrary conclusions on the in situ ozone production, as higher NMHCs would facilitate ozone production by promoting radical cycling, rather than net destruction. Actually, our sensitivity studies showed that the in situ ozone production was not sensitive to NMHCs at WLG (see Fig. 6). Second, the level of hydrogen peroxide (H_2O_2) measured in Ma et al. (2002) was also high with a daily average of 1.6 ppbv, and was attributed to the long-range transport. In the present study, H_2O_2 was not measured but predicted by the model.

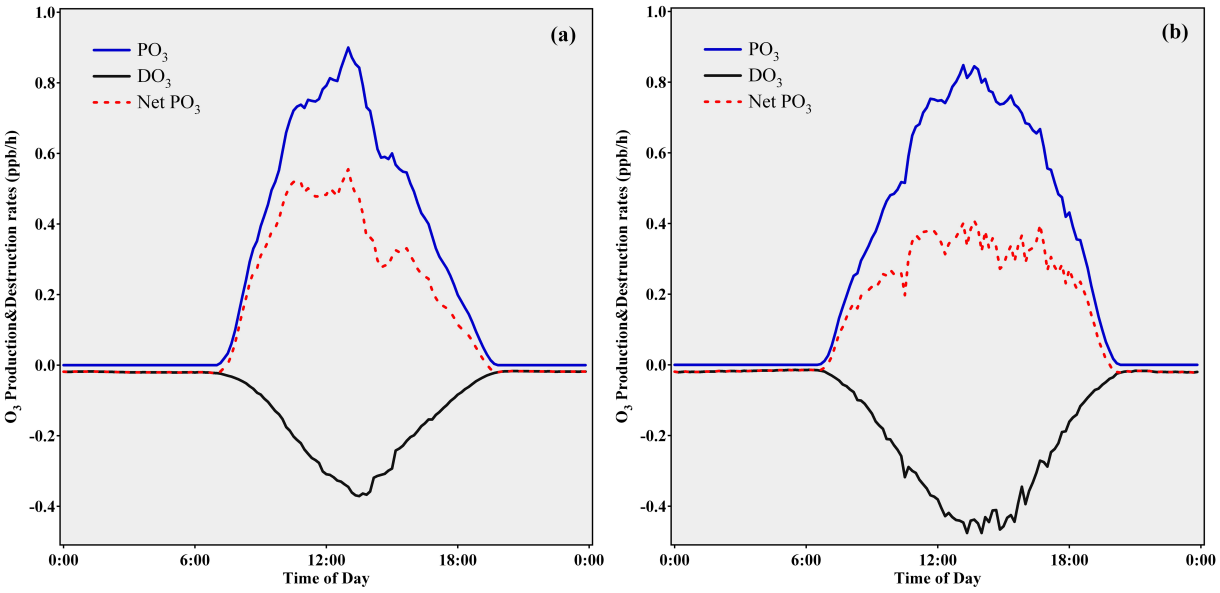

Fig. 4. Modeled O_3 in situ production, destruction, and net rates at WLG in **(a)** spring and **(b)** summer.

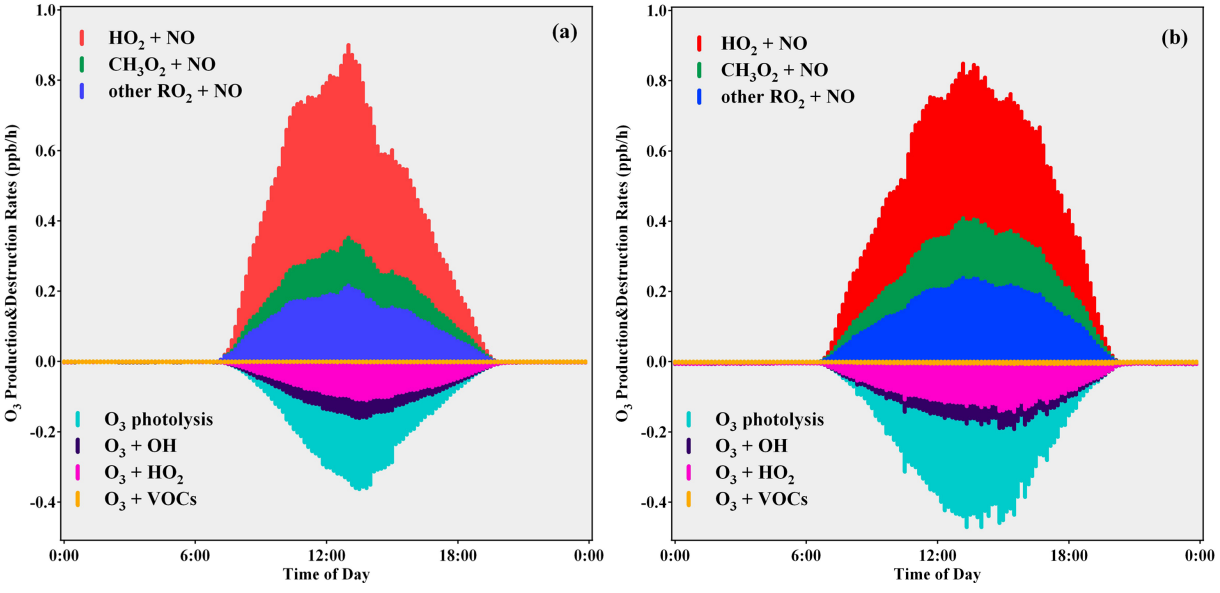

Fig. 5. Breakdown of O_3 in situ production and destruction rates at WLG in **(a)** spring and **(b)** summer.

As the box model did not take transport into account, the model-simulated H_2O_2 should be considered as locally photochemically produced, and was much lower (daily average = 0.38 ppbv) than the previous measurements. This difference should also not be the reason for the different conclusions between two studies, because higher H_2O_2 would enhance ozone production by supplying more OH radicals. We conducted a sensitivity model run with higher H_2O_2 (daily average = 1.6 ppbv) and indeed found a higher net ozone production rate in summer. Third, the level of NO in the previous study was much lower. In Ma et al. (2002), NO was not in situ measured but estimated in the model with constraints of NO_2 which was measured from the filter packs sampling and ion chromatography analysis. The filter measurements showed a NO_2 mixing ratio of 48 ppt with a model-simulated noontime NO level of 13–19 pptv in summer 1996. In comparison, our in situ measurements suggested a much higher level of NO (40–50 pptv) in summer 2003 (note that NO_2 was simulated within the model with constraints of NO, and the mean mixing ratio was 110 pptv in summer). The NO level is usually a key factor in determining the in situ ozone photochemical regime, i.e., production or destruction, at remote

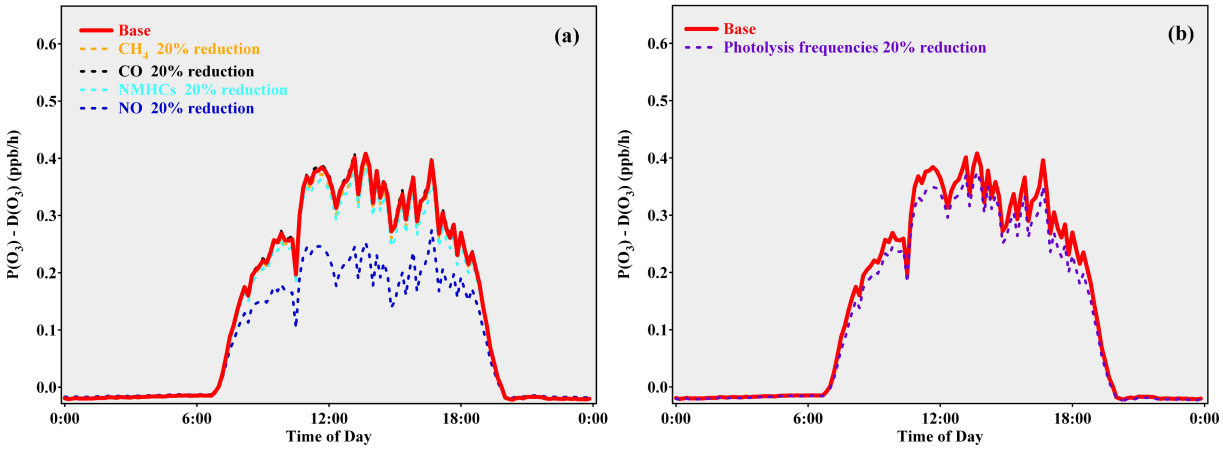

Fig. 6. Sensitivity of summertime O_3 production rates to **(a)** ozone precursors and **(b)** photolysis frequencies at WLG.

locations (Zanis et al., 2000a). We think the difference in NO levels should be the key to the different conclusions between two studies. We also performed a sensitivity model run with lower NO (18 pptv) and indeed found a net ozone destruction (net rate $= -0.03$ ppb h^{-1}) in summer. It is not clear whether the discrepancy in NO levels was due to the interannual variation of trace gas composition or the difference in the method for NO determination in the two studies. Accurate measurements of NO are critical to understanding the exact role of photochemistry in the ozone budget at WLG. Our result is also different from the chemical transport modeling study by Li et al. (2009), which derived a weak ozone destruction (-0.4 ppb day^{-1}) in summer at WLG.

The net ozone production rates determined at WLG in the present study are comparable to those deduced from other remote continental sites with similar NO levels. For instance, Fischer et al. (2003) reported a net ozone production rate of 0.1–0.3 ppb h^{-1} at Mt. Cimone with mean NO levels of the order of 40 pptv during the June 2000 MINATROC campaign. During the FREETEX'96 study at Jungfraujoch in April/May 1996, the daytime net ozone production rates were calculated as 0.27 and 0.13 ppb h^{-1} by a photochemical box model and from the in situ measurements of $HO_2 + RO_2$ (Zanis et al., 2000b). During the following FREETEX'98 in March/April 1998, the experimentally derived net ozone production rates varied from ~ 0.1 ppb h^{-1} for the relatively clean days to > 1 ppb h^{-1} on the more polluted days, with average NO levels of 27 and 261 pptv, respectively (Zanis et al., 2000a). By contrast, net ozone destruction was determined at Mauna Loa, a remote mountainous site in the central North Pacific with very low NO levels. During the MLOPEX2 campaign in 1991/1992, the net ozone production rates were estimated at -0.4–0.8 and -1.4 ppb h^{-1} with mean NO levels of ~ 19 pptv in spring and summer, respectively (Ridley et al., 1998). Note that the North Pacific results are similar to those of Ma et al. (2002), who used similar NO input values.

Figure 5a and b break down the calculated ozone production and destruction rates from individual reaction pathways at WLG in late spring and summer. The partitioning of ozone production and destruction rates was similar in both seasons. Overall, the reaction of HO_2 with NO (R4) dominated the ozone production, with averages of 60 % and 52 % in spring and summer, respectively. The NO oxidation by RO_2 (R3) composed the remainder (40 % and 48 %), with CH_3O_2 alone making a considerable contribution (15 % and 20 %). In terms of ozone destruction, ozone photolysis (R8) contributed the most with means of 48 % and 54 % in spring and summer, followed by the reactions of $O_3 + HO_2$ (R10; 36 % and 33 %) and $O_3 + OH$ (R9; 15 % and 11 %). The ozonolysis of unsaturated VOCs (R11) was only a minor contributor (1.4 % and 2.2 %) to the ozone loss due to the low levels of alkenes at WLG (see Table 1).

A number of sensitivity model runs were conducted to examine the sensitivity of ozone production to ozone precursors and to diagnose the modeling results against initial conditions. Figure 6a shows the responses of net ozone production rates to reductions by 20 % of CO, CH_4, NMHCs, and NO (note that only the summertime results are shown; the results in spring were similar). One can see that the ozone production at WLG was insensitive to CO, CH_4 and NMHCs, but was highly sensitive to NO. A 20 % decrease in NO led to reductions of 28 % and 36 % in net ozone production in spring and summer. This was as expected since ozone production in remote atmospheres is generally in a NO_x-limited regime. Solar radiation affecting photolysis frequencies of various photosensitive species is an important factor in controlling the atmospheric photochemistry and thus ozone formation. In the base runs, the photolysis frequencies were parameterized with the assumption of clear sky conditions (no cloud and aerosol). Sensitivity tests by reducing photolysis rates by 20 % were carried out to examine the potential effects of cloud and/or aerosols on the modeling results. The results indicated that reducing photolysis frequencies could

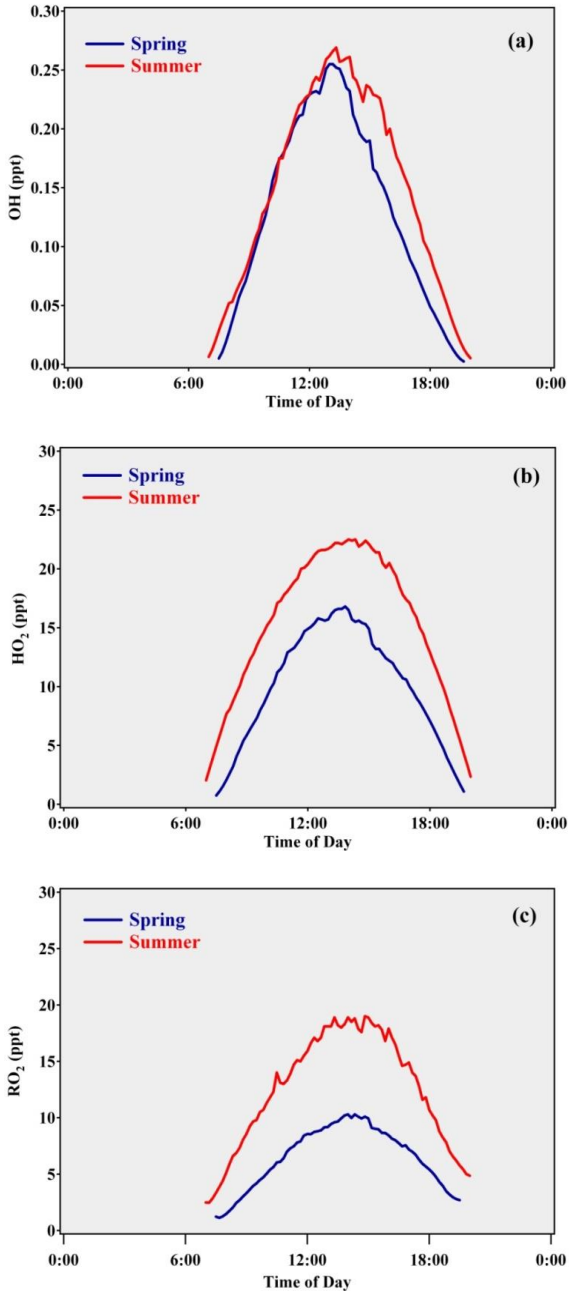

Fig. 7. Model-predicted daytime profiles of **(a)** OH, **(b)** HO_2, and **(c)** RO_2 at WLG.

considerably cut down the net ozone production (13 % in spring and 10 % in summer; see Fig. 6b). Lowering photolysis can attenuate ozone production by reducing the supply of RO_x, which can be compensated in part by weakening the ozone loss by photolysis. Nevertheless, reduction in photolysis frequencies did not change the modeling conclusion that in situ photochemistry led to net ozone production at WLG.

As the boundary layer height was not measured but assumed to vary within general values, sensitivity of the model output was tested by changing the maximum mixing height profiles (i.e., 1000 m and 2000 m). The results indicated that the impacts were negligible (< 2 % of change in net ozone production rates). Given the important potential for the atmospheric oxidative capacity (e.g., Kleffmann et al., 1998; Thornton et al., 2008), the sensitivity of the model results to the heterogeneous processes of HONO formation and HO_2 loss were also tested by turning off these reactions and rerunning the model. The results were < 5 % changes in the net ozone production rates. Hence these processes were found to be less important for the remote environment of WLG under conditions of very low concentrations of NO_x and aerosols.

3.3.2 Radical budget

Figure 7 depicts the modeled daytime profiles of OH, HO_2 and RO_2 at WLG for the spring and summer campaigns. As expected, the concentrations of HO_2 and RO_2 were significantly higher in summer than in late spring, although the OH levels were comparable in both seasons. The midday peak mixing ratios of OH, HO_2 and RO_2 in spring were 0.26, 16.8 and 10.3 pptv, compared to 0.27, 22.5 and 18.9 pptv in summer. Such a seasonal pattern of RO_x is linked with the seasonal behavior of most VOC compounds showing higher springtime and lower summertime concentrations. The peroxy radicals largely existed in the form of HO_2, which was also in line with the result that NO oxidation by HO_2 dominated the ozone production.

The simulated RO_x concentrations at WLG in this study were comparable to those derived from other remote mountainous sites at northern midlatitudes. For example, at Mt. Cimone the measured average midday total peroxy radical ($HO_2 + RO_2$) concentrations were of the order of 30 pptv during the MINATROC campaign conducted in June 2000 (Fischer et al., 2003). At Jungfraujoch, the mean midday levels of peroxy radicals were measured at 13 pptv during the FREETEX'98 in March/April 1998 (Zanis et al., 2000a). At Idaho Hill (USA, 3070 m), average noontime peroxy radical concentrations of 32 pptv were observed during the TOPHE campaign in August/September 1993 (Cantrell et al., 1997). At Mauna Loa, the intensive measurements during the MLOPEX2 in spring and summer 1992 showed average midday peroxy radical levels of 25 pptv (Cantrell et al., 1996). At Izana, the mean noontime concentrations of peroxy radicals were recorded at 65 pptv during the OCTA experiment in July/August 1994 (Fischer et al., 1998).

Table 4 documents the major initiation and termination processes of OH, HO_2, RO_2, and the total RO_x simulated at WLG. Overall, the budgets of RO_x radicals were similar in both seasons, although the reaction rates of most processes were much higher in summer than in spring. Ozone photolysis turned out to be the predominant primary source of OH and also RO_x with daytime average production rates of 172 and 274 ppt h^{-1} in spring and summer, respectively. Photolysis of OVOCs other than formaldehyde

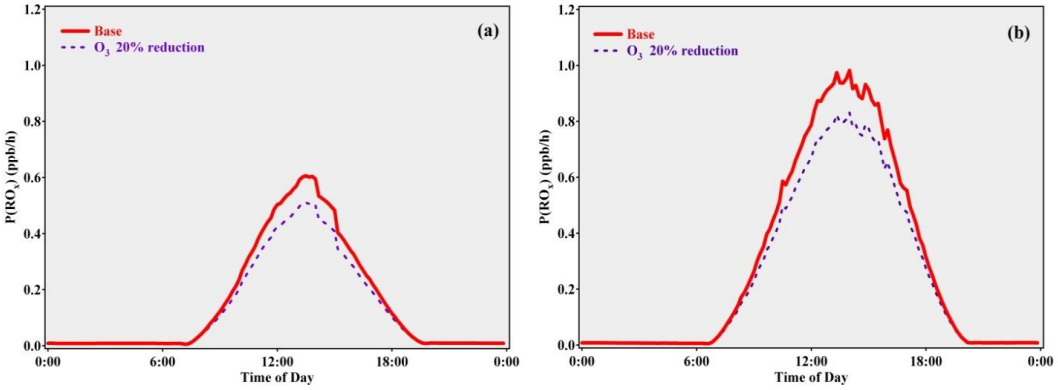

Fig. 8. Sensitivity of RO_x production rates to surface O_3 levels at WLG in **(a)** spring and **(b)** summer.

Table 4. Major initiation and termination processes of RO_x radicals and their contribution as daytime averages at WLG[a].

Chemical process	Spring (07:30–19:30 LT)				Summer (07:00–20:00 LT)			
	OH	HO_2	RO_2	RO_x	OH	HO_2	RO_2	RO_x
Initiation pathways								
O_3 photolysis	172			172	274			274
HONO photolysis	5.6			5.6	3.3			3.3
HNO_3 photolysis[b]	0.1			0.1	0.0			0.0
H_2O_2 photolysis[b]	5.9			5.9	13.3			13.3
HCHO photolysis[b]		48.4		48.4		89.6		89.6
Other OVOCs photolysis	4.2	25.0	31.7	60.9	8.0	60.5	67.7	136
O_3+ VOCs	1.5	0.3	1.3	3.1	2.6	1.8	1.1	5.5
NO_3+ VOCs			1.9	1.9			0.6	0.6
HO_2NO_2 photolysis[c]		0.0		0.0		0.2		0.2
Termination pathways								
OH + NO	3.9			3.9	2.5			2.5
$OH + NO_2$	10.7			10.7	7.4			7.4
$OH + HO_2$	12.5	12.5		25.0	19.0	19.0		38.0
$HO_2 + HO_2$		65.2		65.2		134		134
$HO_2 + RO_2$		52.0	52.0	104		103	103	206
HO_2 heterogeneous loss		5.5		5.5		8.4		8.4
$RO_2 + RO_2$			1.6	1.6			6.4	6.4
$RO_2 + NO = RONO_2$			4.4	4.4			4.0	4.0
$RO_2 + NO_2$[d]			29.5	29.5			23.2	23.2

[a] Units are ppt h^{-1}. [b] The model-simulated average HNO_3, H_2O_2, and HCHO were 46 (30) pptv, 0.18 (0.38) ppbv, and 0.29 (0.53) ppbv in spring (summer), respectively. [c] The formation rate of HO_2NO_2 from HO_2 and NO_2 has been subtracted. [d] The formation rates of RO_2 from PANs decomposition have been subtracted.

(HCHO) was the second largest source of RO_x mainly contributing to HO_2 (25.0 and 60.5 ppt h^{-1}) and RO_2 (31.7 and 67.7 ppt h^{-1}). HCHO photolysis was the third important source of RO_x, and also the largest source of HO_2 (48.4 and 89.6 ppt h^{-1}). It should be pointed out that the HCHO and OVOCs in the present study were only of local photochemical origin since the box model cannot take transport into account. The model-simulated average HCHO concentrations were 0.29 ppbv in spring and 0.53 ppbv in summer, respectively. Previous measurements from a 10 days campaign in August–September 2005 showed very high levels of HCHO (average = 4.16 ppbv) and CH_3CHO (average = 4.25 ppbv) at WLG (Mu et al., 2007). Such high levels of carbonyls were usually observed in polluted suburban or rural environments, but were rarely measured at remote sites. If this was also the case in the present study, HCHO would take over ozone as the predominant radical source as indicated by our sensitivity analysis (620 ppt h^{-1}). Further accurate measurements of HCHO (and other OVOCs) are required to check this issue and understand the sources of OVOCs

at WLG. The fourth important RO_x supplier at WLG was the photolysis of H_2O_2 with average daytime OH production of 5.9 and 13.3 ppt h^{-1} in spring and in summer. As stated above, the model-simulated H_2O_2 (mean = 0.38 ppbv in summer) was also lower than the previous measurements (mean = 1.6 ppbv; Ma et al., 2002). However, we conducted a sensitivity model run with that high H_2O_2 levels and found the ranking remained (53 ppt h^{-1} of OH production). Other initiation processes that may be important in polluted regions, such as HONO photolysis, ozonolysis of alkenes, and reactions of NO_3+VOCs, contributed little to the primary RO_x production at WLG. The ultimate loss of radicals was dominated by the self and cross reactions among HO_2, RO_2 and OH, which consumed RO_x on average at 196 and 384 ppt h^{-1} during the daytime in spring and in summer. In comparison, reactions of RO_x+NO_x contributed only 48.5 and 37.1 ppt h^{-1} to the net radical losses during both campaigns. Furthermore, the heterogeneous loss of HO_2 on aerosols was negligible due to the very low aerosol loadings at WLG.

As indicated above, photolysis of O_3 presents the dominant primary source of RO_x at WLG. This implies strong feedback of O_3 to the photochemistry of this natural atmosphere. To quantify the impact of O_3 on the atmospheric oxidative capacity, sensitivity model runs were conducted by reducing ozone levels to examine the response of RO_x production. The results are shown in Fig. 8. As expected, reduction in surface O_3 (i.e., 20 %) at WLG would result in significant decreases in the RO_x production rate (i.e., 14.5 % in spring and 14.8 % in summer). The ozone burden at WLG is primarily controlled by regional transport of the photochemically produced ozone from upwind regions (mainly central and eastern China), downward transport of stratospheric air, and in situ photochemistry (Wang et al., 2006; Ding and Wang, 2006; Li et al., 2009). Our previous study had indicated the dominant contribution of pollution transport from central/eastern China to the summertime surface ozone at WLG (Xue et al., 2011); the present study reveals that ozone is the dominant source of RO_x radicals, the principal oxidants in the atmosphere. These findings altogether suggest that pollution transport from central and eastern China may influence the chemistry of the background atmosphere over the Qinghai-Tibetan Plateau.

4 Summary and conclusions

Concurrent measurements of VOCs, NO, other related trace gases and meteorological parameters were made during two intensive campaigns in late spring and summer 2003 at WLG, a baseline observatory on the Qinghai-Tibetan Plateau. Most VOC species presented a seasonal pattern with higher springtime and lower summertime concentrations and a diurnal variation with higher nighttime and lower daytime values. During the campaigns, the site received air masses from the remote central Eurasian continent, from Mongolia and inland northern China, from central southern China, and from India and southwestern China, all of which showed distinct VOC speciation. The air masses from the central Eurasian continent had the lowest levels of VOCs compared to those having passed over the China or Indian subcontinent.

This study provided an opportunity to better understand the role of in situ photochemistry in the chemical ozone budget at WLG, a topic currently still of some debate. Our results based on an observation-constrained photochemical box model suggest net ozone production due to the in situ photochemistry in both spring and summer. This was different from the previous studies that suggested net ozone destruction in summer at WLG. The difference in NO levels seemed to be the key factor leading to different conclusions. Ozone was primarily produced by the oxidation of NO by HO_2 (and also RO_2), and was mainly destroyed via photolysis and reactions with OH and HO_2. The RO_x radical budget was also evaluated. Ozone photolysis was the dominant primary source of RO_x, followed by the photolysis of secondary OVOCs and hydrogen peroxide. The radical loss was governed by the self and cross reactions of HO_2 and RO_2. The origins and photochemistry of VOCs obtained in the present study are useful to constrain/validate regional and global chemical transport models, and to yield scientific insights into the human perturbation of the natural atmosphere over this globally unique landmass. Indeed, our results (in combination with our previous study) suggest that transport of anthropogenic pollution from central and eastern China may perturb the chemistry of the background atmosphere over the plateau.

Acknowledgements. The authors would like to thank Steven Poon and Anson Wong for their contribution to the field studies, and Aijun Ding for his helpful suggestion. We are grateful to the staff at the WLG Observatory for their assistance throughout the field campaigns, to the Master Chemical Mechanism group at University of Leeds for providing the mechanism, and to NOAA Air Resources Laboratory (ARL) for providing the HYSPLIT model and meteorological data. We also thank the two anonymous reviewers for their helpful comments to improve the original manuscript. The field measurements at WLG were supported by the Hong Kong Research Grants Council (PolyU5057/02E), and the data analysis was funded by the Norwegian Research Council (SOGG-EA, 193774) and the Hong Kong Polytechnic University (1-BB94).

Edited by: T. Butler

References

Akimoto, H., Mukai, H., Nishikawa, M., Murano, K., Hatakeyama, S., Liu, C. M., Buhr, M., Hsu, K. J., Jaffe, D. A., Zhang, L., Honrath, R., Merrill, J. T., and Newell, R. E.: Long-range transport of ozone in the East Asian Pacific rim region, J. Geophys. Res.-Atmos., 101, 1999–2010, 1996.

Atlas, E. L. and Ridley, B. A.: The Mauna Loa observatory photochemistry experiment: introduction, J. Geophys. Res.-Atmos., 101, 14531–14541, 1996.

Berntsen, T. K., Karlsdottir, S., and Jaffe, D. A.: Influence of Asian emissions on the composition of air reaching the North Western United States, Geophys. Res. Lett., 26, 2171–2174, 1999.

Blake, D. R., Smith, T. W., Chen, T. Y., Whipple, W. J., and Rowland, F. S.: Effects of biomass burning on summertime nonmethane hydrocarbon concentrations in the Canadian wetlands, J. Geophys. Res.-Atmos., 99, 1699–1719, 1994.

Blake, N. J., Blake, D. R., Simpson, I. J., Meinardi, S., Swanson, A. L., Lopez, J. P., Katzenstein, A. S., Barletta, B., Shirai, T., Atlas, E., Sachse, G., Avery, M., Vay, S., Fuelberg, H. E., Kiley, C. M., Kita, K., and Rowland, F. S.: NMHCs and halocarbons in Asian continental outflow during the Transport and Chemical Evolution over the Pacific (TRACE-P) field campaign: comparison with PEM-West B, J. Geophys. Res.-Atmos., 108, 8516, doi:10.1029/2002JD002490, 2003.

Cantrell, C. A., Shetter, R. E., Gilpin, T. M., and Calvert, J. G.: Peroxy radicals measured during Mauna Loa observatory photochemistry experiment 2: the data and first analysis, J. Geophys. Res.-Atmos., 101, 14643–14652, 1996.

Cantrell, C. A., Shetter, R. E., Calvert, J. G., Eisele, F. L., Williams, E., Baumann, K., Brune, W. H., Stevens, P. S., and Mather, J. H.: Peroxy radicals from photostationary state deviations and steady state calculations during the Tropospheric OH Photochemistry Experiment at Idaho Hill, Colorado, 1993, J. Geophys. Res.-Atmos., 102, 6369–6378, 1997.

Carpenter, L. J., Green, T. J., Mills, G. P., Bauguitte, S., Penkett, S. A., Zanis, P., Schuepbach, E., Schmidbauer, N., Monks, P. S., and Zellweger, C.: Oxidized nitrogen and ozone production efficiencies in the springtime free troposphere over the Alps, J. Geophys. Res.-Atmos., 105, 14547–14559, 2000.

Crutzen, P.: Discussion of chemistry of some minor constituents in stratosphere and troposphere, Pure Appl. Geophys., 106, 1385–1399, 1973.

Crutzen, P.: Ozone in the troposphere, in Composition, Chemistry and Climate of the Atmosphere, edited by: Singh, H. B., Van Nostrand Reinhold, New York, 1995.

Ding, A. J. and Wang, T.: Influence of stratosphere-to-troposphere exchange on the seasonal cycle of surface ozone at Mount Waliguan in western China, Geophys. Res. Lett., 33, L03803, doi:10.1029/2005GL024760, 2006.

Edwards, P., Evans, M. J., Commane, R., Ingham, T., Stone, D., Mahajan, A. S., Oetjen, H., Dorsey, J. R., Hopkins, J. R., Lee, J. D., Moller, S. J., Leigh, R., Plane, J. M. C., Carpenter, L. J., and Heard, D. E.: Hydrogen oxide photochemistry in the northern Canadian spring time boundary layer, J. Geophys. Res.-Atmos., 116, D22306, doi:10.1029/2011JD016390, 2011.

Fischer, H., Nikitas, C., Parchatka, U., Zenker, T., Harris, G. W., Matuska, P., Schmitt, R., Mihelcic, D., Muesgen, P., Paetz, H. W., Schultz, M., and Volz-Thomas, A.: Trace gas measurements during the Oxidizing Capacity of the Tropospheric Atmosphere campaign 1993 at Izana, J. Geophys. Res.-Atmos., 103, 13505–13518, 1998.

Fischer, H., Kormann, R., Klüpfel, T., Gurk, Ch., Königstedt, R., Parchatka, U., Mühle, J., Rhee, T. S., Brenninkmeijer, C. A. M., Bonasoni, P., and Stohl, A.: Ozone production and trace gas correlations during the June 2000 MINATROC intensive measurement campaign at Mt. Cimone, Atmos. Chem. Phys., 3, 725–738, doi:10.5194/acp-3-725-2003, 2003.

Gangoiti, G., Albizuri, A., Alonso, L., Navazo, M., Matabuena, M., Valdenebro, V., García, J. A., and Millán, M. M.: Subcontinental transport mechanisms and pathways during two ozone episodes in northern Spain, Atmos. Chem. Phys., 6, 1469–1484, doi:10.5194/acp-6-1469-2006, 2006.

Guenther, A.: Seasonal and spatial variations in natural volatile organic compound emissions, Ecolog. Appl., 7, 34–45, 1997.

Guo, H., Wang, T., Blake, D. R., Simpson, I. J., Kwok, Y. H., and Li, Y. S.: Regional and local contributions to ambient non-methane volatile organic compounds at a polluted rural/coastal site in Pearl River Delta, China, Atmos. Environ., 40, 2345–2359, 2006.

HTAP, Hemospheric transport of air pollution, Part A: ozone and particulate matter, New York and Geneva, 2010 (http://www.htap.org/).

Hayman, G. D.: Effects of pollution control on UV exposure, AEA Technology Final Report prepared for the Department of Health and Contract 121/6377, AEA Technology, Oxfordshire, UK, 1997.

Jacob, D. J., Logan, J. A., and Murti, P. P.: Effect of rising Asian emissions on surface ozone in the United States, Geophys. Res. Lett., 26, 2175–2178, 1999.

Jacob, D. J., Crawford, J. H., Kleb, M. M., Connors, V. S., Bendura, R. J., Raper, J. L., Sachse, G. W., Gille, J. C., Emmons, L., and Heald, C. L.: Transport and Chemical Evolution over the Pacific (TRACE-P) aircraft mission: design, execution, and first results, J. Geophys. Res.-Atmos., 108, 1–19, 2003.

Jaffe, D., Anderson, T., Covert, D., Kotchenruther, R., Trost, B., Danielson, J., Simpson, W., Berntsen, T., Karlsdottir, S., Blake, D., Harris, J., Carmichael, G., and Uno, I.: Transport of Asian air pollution to North America, Geophys. Res. Lett., 26, 711–714, 1999.

Jenkin, M. E., Saunders, S. M., Derwent, R. G., and Pilling, M. J.: Construction and application of a master chemical mechanism (MCM) for modelling tropospheric chemistry., Abstr. Pap. Am. Chem. S., 214, 116-COLL, 1997.

Jenkin, M. E., Saunders, S. M., Wagner, V., and Pilling, M. J.: Protocol for the development of the Master Chemical Mechanism, MCM v3 (Part B): tropospheric degradation of aromatic volatile organic compounds, Atmos. Chem. Phys., 3, 181–193, doi:10.5194/acp-3-181-2003, 2003.

Kivekäs, N., Sun, J., Zhan, M., Kerminen, V.-M., Hyvärinen, A., Komppula, M., Viisanen, Y., Hong, N., Zhang, Y., Kulmala, M., Zhang, X.-C., Deli-Geer, and Lihavainen, H.: Long term particle size distribution measurements at Mount Waliguan, a high-altitude site in inland China, Atmos. Chem. Phys., 9, 5461–5474, doi:10.5194/acp-9-5461-2009, 2009.

Kleffmann, J., Becker, K. H., and Wiesen, P.: Heterogeneous NO_2 conversion processes on acid surfaces: possible atmospheric implications, Atmos. Environ., 32, 2721–2729, 1998.

Klemp, D., Kley, D., Kramp, F., Buers, H. J., Pilwat, G., Flocke, F., Patz, H. W., and VolzThomas, A.: Long-term measurements of light hydrocarbons (C_2-C_5) at Schauinsland (Black Forest), J. Atmos. Chem., 28, 135–171, 1997.

Li, G., Lei, W., Zavala, M., Volkamer, R., Dusanter, S., Stevens, P., and Molina, L. T.: Impacts of HONO sources on the photochemistry in Mexico City during the MCMA-2006/MILAGO Campaign, Atmos. Chem. Phys., 10, 6551–6567, doi:10.5194/acp-10-

6551-2010, 2010.

Li, J., Wang, Z. F., Akimoto, H., Tang, J., and Uno, I.: Modeling of the impacts of China's anthropogenic pollutants on the surface ozone summer maximum on the northern Tibetan Plateau, Geophys. Res. Lett., 36, L24802, doi:10.1029/2009GL041123, 2009.

Lin, M., Holloway, T., Oki, T., Streets, D. G., and Richter, A.: Multi-scale model analysis of boundary layer ozone over East Asia, Atmos. Chem. Phys., 9, 3277–3301, doi:10.5194/acp-9-3277-2009, 2009.

Lin, M., Holloway, T., Carmichael, G. R., and Fiore, A. M.: Quantifying pollution inflow and outflow over East Asia in spring with regional and global models, Atmos. Chem. Phys., 10, 4221–4239, doi:10.5194/acp-10-4221-2010, 2010.

Lin, M., Fiore, A. M., Horowitz, W., Cooper, O. R., Naik, V., Holloway, J., Johnson, B. J., Middlebrook, A. M., Oltmans, S. J., Pollack, I. B., Ryerson, T. B., Warner, J. X., Wiedinmyer, C., Wilson, J., and Wyman, B: Transport of Asian ozone pollution into surface air over the western United States in spring, J. Geophys. Res.-Atmosphere, 117, D00V07, doi:10.1029/2011JD016961, 2012.

Ma, J. Z., Tang, J., Zhou, X. J., and Zhang, X. S.: Estimates of the chemical budget for ozone at Waliguan Observatory, J. Atmos. Chem., 41, 21–48, 2002.

Ma, J. Z., Tang, J., Li, S. M., and Jacobson, M. Z.: Size distributions of ionic aerosols measured at Waliguan Observatory: implication for nitrate gas-to-particle transfer processes in the free troposphere, J. Geophys. Res.-Atmos., 108, 4541, doi:10.1029/2002JD003356, 2003.

Ma, J. Z., Zheng, X. D., and Xu, X. D.: Comment on "Why does surface ozone peak in summertime at Waliguan?" by Zhu, B., Akimoto, H., Wang, Z., Sudo, K., Tang, J., and Uno, I., Geophys. Res. Lett., 32, L01805, doi:10.1029/2004GL021683, 2005.

Monks, P. S.: A review of the observations and origins of the spring ozone maximum, Atmos. Environ., 34, 3545–3561, 2000.

Morikawa, T., Wakamatsu, S., Tanaka, M., Uno, I., Kamiura, T., and Maeda, T.: C_2-C_5 hydrocarbon concentrations in central Osaka, Atmos. Environ., 32, 2007–2016, 1998.

Mu, Y., Pang, X., Quan, J., and Zhang, X.: Atmospheric carbonyl compounds in Chinese background area: a remote mountain of the Qinghai-Tibetan Plateau, J. Geophys. Res.-Atmosphere, 112, D22302, doi:10.1029/2006JD008211, 2007.

National Research Council: Rethinking the ozone problem in urban and regional air pollution, Natl. Acad. Press, Washington, DC, 1991.

Ridley, B., Walega, J., Hubler, G., Montzka, D., Atlas, E., Hauglustaine, D., Grahek, F., Lind, J., Campos, T., Norton, R., Greenberg, J., Schauffler, S., Oltmans, S., and Whittlestone, S.: Measurements of NO_x and PAN and estimates of O_3 production over the seasons during Mauna Loa Observatory Photochemistry Experiment 2, J. Geophys. Res.-Atmos., 103, 8323–8339, 1998.

Rudolph, J.: The tropospheric distribution and budget of ethane, J. Geophys. Res.-Atmos., 100, 11369–11381, 1995.

Russo, R. S., Talbot, R. W., Dibb, J. E., Scheuer, E., Seid, G., Jordan, C. E., Fuelberg, H. E., Sachse, G. W., Avery, M. A., Vay, S. A., Blake, D. R., Blake, N. J., Atlas, E., Fried, A., Sandholm, S. T., Tan, D., Singh, H. B., Snow, J., and Heikes, B. G.: Chemical composition of Asian continental outflow over the western Pacific: results from Transport and Chemical Evolution over the Pacific (TRACE-P), J. Geophys. Res.-Atmos., 108, 8804, doi:10.1029/2002JD003184, 2003.

Saunders, S. M., Jenkin, M. E., Derwent, R. G., and Pilling, M. J.: Protocol for the development of the Master Chemical Mechanism, MCM v3 (Part A): tropospheric degradation of non-aromatic volatile organic compounds, Atmos. Chem. Phys., 3, 161–180, doi:10.5194/acp-3-161-2003, 2003.

Sharma, U. K., Kajii, Y., and Akimoto, H.: Seasonal variation of C_2–C_6 NMHCs at Happo, a remote site in Japan, Atmos. Environ., 34, 4447–4458, 2000.

Simpson, I. J., Blake, N. J., Barletta, B., Diskin, G. S., Fuelberg, H. E., Gorham, K., Huey, L. G., Meinardi, S., Rowland, F. S., Vay, S. A., Weinheimer, A. J., Yang, M., and Blake, D. R.: Characterization of trace gases measured over Alberta oil sands mining operations: 76 speciated C_2-C_10 volatile organic compounds (VOCs), CO_2, CH_4, CO, NO, NO_2, NO_y, O_3 and SO_2, Atmos. Chem. Phys., 10, 11931–11954, doi:10.5194/acp-10-11931-2010, 2010.

Stohl, A., Bonasoni, P., Cristofanelli, P., Collins, W., Feichter, J., Frank, A., Forster, C., Gerasopoulos, E., Gaggeler, H., James, P., Kentarchos, T., Kromp-Kolb, H., Kruger, B., Land, C., Meloen, J., Papayannis, A., Priller, A., Seibert, P., Sprenger, M., Roelofs, G. J., Scheel, H. E., Schnabel, C., Siegmund, P., Tobler, L., Trickl, T., Wernli, H., Wirth, V., Zanis, P., and Zerefos, C.: Stratosphere-troposphere exchange: a review, and what we have learned from STACCATO, J. Geophys. Res.-Atmos., 108, 8526, doi:10.1029/2002JD00227, 2003.

Suthawaree, J., Kato, S., Okuzawa, K., Kanaya, Y., Pochanart, P., Akimoto, H., Wang, Z., and Kajii, Y.: Measurements of volatile organic compounds in the middle of Central East China during Mount Tai Experiment 2006 (MTX2006): observation of regional background and impact of biomass burning, Atmos. Chem. Phys., 10, 1269–1285, doi:10.5194/acp-10-1269-2010, 2010.

Tang, J., Wen, Y. P., Xu, X. B., Zheng, X. D., Guo, S., and Zhao, Y. C.: China Global Atmosphere Watch Baseline Observatory and its measurement program, in CAMS Annural Report 1994-95, China Meteorol. Press, Beijing, 56–65, 1995.

Thornton, J. A., Jaegle, L., and McNeill, V. F.: Assessing known pathways for HO_2 loss in aqueous atmospheric aerosols: regional and global impacts on tropospheric oxidants, J. Geophys. Res.-Atmos., 113, D05303, doi:10.1029/2007JD009236, 2008.

Wang, C. J. L., Blake, D. R., and Rowland, F. S.: Seasonal variations in the atmospheric distribution of a reactive chlorine compound, tetrachloroethene ($CCl_2 =CCl_2$), Geophys. Res. Lett., 22, 1097–1100, 1995.

Wang, T., Wong, H. L. A., Tang, J., Ding, A., Wu, W. S., and Zhang, X. C.: On the origin of surface ozone and reactive nitrogen observed at a remote mountain site in the northeastern Qinghai-Tibetan Plateau, western China, J. Geophys. Res.-Atmos., 111, D08303, doi:10.1029/2005JD006527, 2006.

Wild, O., Pochanart, P., and Akimoto, H.: Trans-Eurasian transport of ozone and its precursors, J. Geophys. Res.-Atmos., 109, D11302, doi:10.1029/2003JD004501, 2004.

Xue, L. K., Wang, T., Zhang, J. M., Zhang, X. C., Deliger, Poon, C. N., Ding, A. J., Zhou, X. H., Wu, W. S., Tang, J., Zhang, Q. Z., and Wang, W. X.: Source of surface ozone and reactive nitrogen speciation at Mount Waliguan in western China: new insights from the 2006 summer study, J. Geophys. Res.-Atmos., 116, D07306, doi:10.1029/2010JD014735, 2011.

Zanis, P., Monks, P. S., Schuepbach, E., Carpenter, L. J., Green, T. J., Mills, G. P., Bauguitte, S., and Penkett, S. A.: In-situ ozone production under free tropospheric conditions during FREETEX '98 in the Swiss Alps, J. Geophys. Res.-Atmos., 105, 24223–24234, 2000a.

Zanis, P., Monks, P. S., Schuepbach, E., and Penkett, S. A.: The role of in-situ photochemistry in the control of ozone during spring at the Jungfraujoch (3,580 m a.s.l.) – comparison of model results with measurements, J. Atmos. Chem., 37, 1–27, 2000b.

Zaveri, R. A., Saylor, R. D., Peters, L. K., Mcnider, R., and Song, A.: A model investigation of summertime diurnal ozone behavior in rural mountainous locations, Atmos. Environ., 29, 1043–1065, 1995.

Zellweger, C., Ammann, M., Buchmann, B., Hofer, P., Lugauer, M., Ruttimann, R., Streit, N., Weingartner, E., and Baltensperger, U.: Summertime NO_y speciation at the Jungfraujoch, 3580 m above sea level, Switzerland, J. Geophys. Res.-Atmos., 105, 6655–6667, 2000.

Zhang, L., Brook, J. R., and Vet, R.: A revised parameterization for gaseous dry deposition in air-quality models, Atmos. Chem. Phys., 3, 2067–2082, doi:10.5194/acp-3-2067-2003, 2003.

Zhang, Q., Streets, D. G., Carmichael, G. R., He, K. B., Huo, H., Kannari, A., Klimont, Z., Park, I. S., Reddy, S., Fu, J. S., Chen, D., Duan, L., Lei, Y., Wang, L. T., and Yao, Z. L.: Asian emissions in 2006 for the NASA INTEX-B mission, Atmos. Chem. Phys., 9, 5131–5153, doi:10.5194/acp-9-5131-2009, 2009.

Zhou, L. X., Tang, J., Wen, Y. P., Li, J. L., Yan, P., and Zhang, X. C.: The impact of local winds and long-range transport on the continuous carbon dioxide record at Mount Waliguan, China, Tellus B, 55, 145–158, 2003.

Zhou, L. X., Worthy, D. E. J., Lang, P. M., Ernst, M. K., Zhang, X. C., Wen, Y. P., and Li, J. L.: Ten years of atmospheric methane observations at a high elevation site in Western China, Atmos. Environ., 38, 7041–7054, 2004.

Zhu, B., Akimoto, H., Wang, Z., Sudo, K., Tang, J., and Uno, I.: Why does surface ozone peak in summertime at Waliguan?, Geophys. Res. Lett., 31, L17104, doi:10.1029/2004GL020609, 2004.